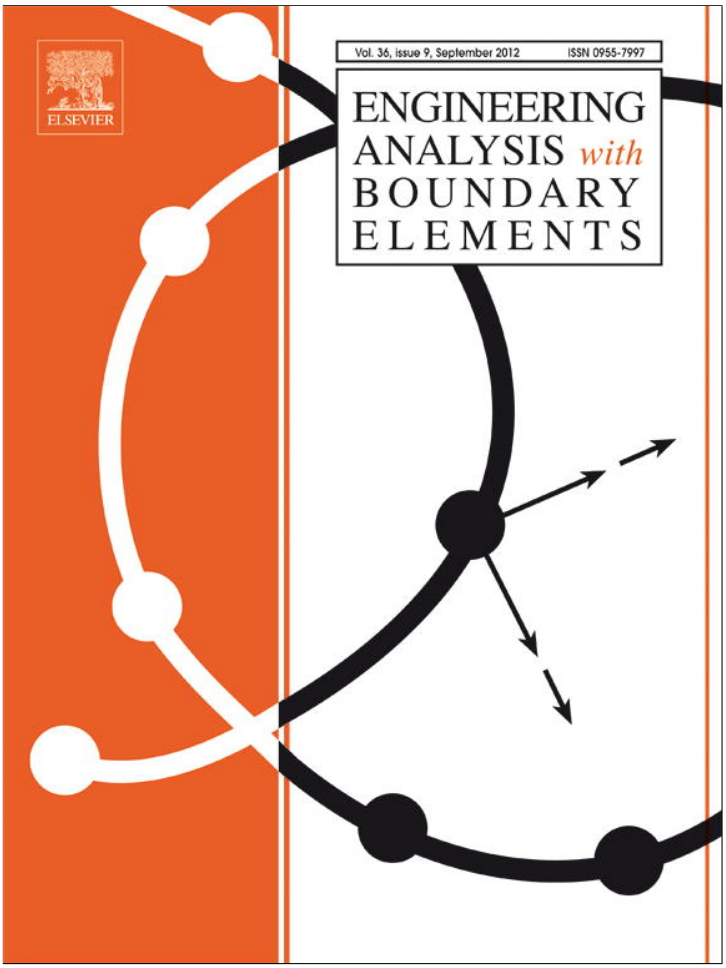

Engineering Analysis with Boundary Elements 36 (2012) 1406–1415

Contents lists available at SciVerse ScienceDirect

Engineering Analysis with Boundary Elements

journal homepage: www.elsevier.com/locate/enganabound

Three-dimensional extended displacement discontinuity method for vertical cracks in transversely isotropic piezoelectric media

MingHao Zhao [a,b,*], RongLi Zhang [b], CuiYing Fan [a], Ernian Pan [a,c]

[a] The School of Mechanical Engineering, Zhengzhou University, No. 100 Science Road, Zhengzhou, Henan Province 450001, PR China
[b] Department of Engineering Mechanics, Zhengzhou University, Zhengzhou, Henan 450001, China
[c] Department of Civil Engineering, University of Akron, Akron, OH 44325, USA

ARTICLE INFO

Article history:
Received 14 February 2011
Accepted 23 September 2011
Available online 10 April 2012

Keywords:
Piezoelectric medium
Displacement discontinuity method
Extended Green's function
Boundary integral equation
Vertical crack
Extended field intensity factor

ABSTRACT

The conventional displacement discontinuity method is extended to study a vertical crack under electrically impermeable condition, running parallel to the poling direction and normal to the plane of isotropy in three-dimensional transversely isotropic piezoelectric media. The extended Green's functions specifically for extended point displacement discontinuities are derived based on the Green's functions of extended point forces and the Somigliana identity. The hyper-singular displacement discontinuity boundary integral equations are also derived. The asymptotical behavior near the crack tips along the crack front is studied and the ordinary 1/2 singularity is obtained at the tips. The extended field intensity factors are expressed in terms of the extended displacement discontinuity on crack faces. Numerical results on the extended field intensity factors for a vertical square crack are presented using the proposed extended displacement discontinuity method.

1. Introduction

Owing to the coupling effects between mechanical and electric properties, piezoelectric materials are finding more and more applications in modern technological fields such as electronics, lasers, supersonics, sensors, actuators, transducers and microwaves [1,2]. In practice, however, defects (such as inclusion, void/crack, etc.) in such materials and related structures are unavoidable and these defects greatly affect the integrity and reliability of the structures. For this reason, analysis of cracks in piezoelectric materials has been always important [3–10].

For some piezoelectric materials, when temperature is higher than the Curie point, spontaneous polarization phenomenon occurs and the hysteresis loop of the polarization P versus the electric field strength E also occurs; meanwhile, the formative aligned electric dipoles remain in the material microstructure. Therefore, the linear constitutive relationship is concerned with the poling direction, and, thus, different poling directions affect the material properties and fracture behavior. A conductive crack (with the crack cavity filled with silver paint) with different poling direction under purely electric loading was studied in [11]. Results showed that the direction of the electric field and the poling direction both could affect the fracture and breakdown resistance of piezoelectric materials. For an arbitrarily oriented crack in a piezoelectric medium [12], the polarization direction plays an important role in the fracture behavior of piezoelectric materials. By carrying out a four-point bending test on a specimen with cracks parallel, perpendicular and inclined to the poling direction under both mechanical and electric field loadings, Banks-Sills et al. [13] and Motola et al. [14] showed that neglecting the piezoelectric effect in calculating stress intensity factors may lead to errors. For a crack normal to the poling direction of a two-dimensional (2D) ferroelectric ceramics [15], crack growth can be retarded under electric and mechanical loadings. There are numerous studies on cracks lying within the plane of isotropy in three-dimensional (3D) transversely isotropic piezoelectric media [16–26]. However, the corresponding problem where the cracks are normal to the isotropic plane has never been investigated. This motivates the work presented in this paper.

The displacement discontinuity boundary integral equation method or boundary element method proposed by Crouch [27] has been demonstrated to be a good framework in handling fractures in elastic and piezoelectric media [6,19,22,25–28]. In the boundary element method [28–34], an important role is played by the Green's function corresponding to a point force or displacement discontinuity. In the present paper, the method proposed by Zhao et al. [35] is extended to derive the extended displacement discontinuity fundamental solutions for the case where a crack is vertical to the isotropic plane and parallel to the electric poling directions in a 3D transversely isotropic piezoelectric medium. These fundamental solutions are then applied to

* Corresponding author at: The School of Mechanical Engineering, Zhengzhou University, No. 100 Science Road, Zhengzhou, Henan Province 450001, PR China. Tel.: +86 371 67781752.
E-mail addresses: memhzhao@zzu.edu.cn, memhzhao@sina.com (M. Zhao).

0955-7997/$ - see front matter © 2012 Elsevier Ltd. All rights reserved.
doi:10.1016/j.enganabound.2012.03.005

obtain the boundary integral equations, and calculate the extended field intensity factors of an arbitrarily vertical crack in terms of the extended displacement discontinuity on the crack face. The extended displacement discontinuity boundary element method is also presented, and the finite element method is further utilized to verify the accuracy of the developed method.

2. Basic equations

In the absence of the body force and electric charge, for a 3D piezoelectric medium with the poling direction along the z-axis in the Cartesian coordinates (x, y, z), the equilibrium equations, Eq. (1a), the kinematic equations, Eq. (1b), and the constitutive equations, Eq. (2), are given as [4,6]

$$\sigma_{ij,j}=0, \quad D_{i,i}=0, \tag{1a}$$

$$\varepsilon_{ij}=\tfrac{1}{2}(u_{i,j}+u_{j,i}), \quad E_i=-\varphi_{,i}, \tag{1b}$$

$$\sigma_{ij}=C_{ijkl}\varepsilon_{kl}-e_{kij}E_k, \tag{2a}$$

$$D_i=e_{ikl}\varepsilon_{kl}+\kappa_{ik}E_k, \tag{2b}$$

where σ_{ij}, ε_{ij}, D_i and E_i denote the stress, strain, electric displacement and electric field strength, respectively; u_i and φ are the elastic displacements and electric potential, respectively; and C_{ijkl}, e_{ijk} and κ_{ij} stand, respectively, for the elastic, piezoelectric and dielectric coefficients.

3. Boundary integral expressions of extended displacements

For a transversely isotropic piezoelectric infinite medium, we again set up the Cartesian coordinate system $oxyz$ such that the plane of isotropy coincides with the oxy plane, and the poling direction is along the z-direction. An arbitrarily-shaped vertical crack S lies in the oyz plane, as shown in Fig. 1. The two faces of the crack S are denoted by S^+ and S^-, respectively. The outward normal vectors of S^+ and S^- are respectively given by

$$\{n_i\}_{S^+}=\{-1,0,0\}, \quad \{n_i\}_{S^-}=\{1,0,0\}. \tag{3}$$

Then, making use of the extended point-force Green's functions [36] and the Somigliana identity for piezoelectric media [37], the elastic displacements and the electric potential at any

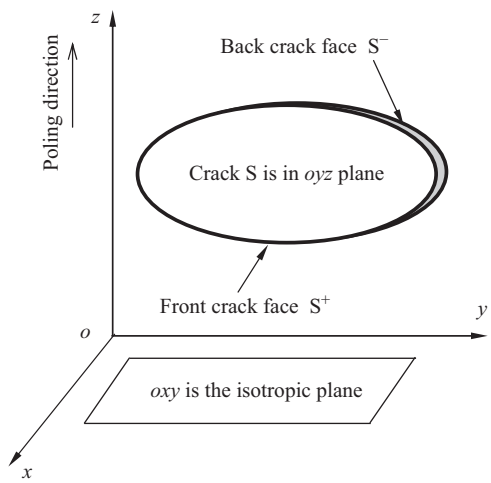

Fig. 1. A transversely isotropic piezoelectric infinite medium with an arbitrarily-shaped crack in the oyz plane.

internal point (x, y, z) can be expressed by the following integrals:

$$u_i(x,y,z)=-\int_{S^+}[P_{ij}^{F}\|u_j\|+\Omega_i^{F}\|\varphi\|]\,dS,$$
$$-\varphi(x,y,z)=-\int_{S^+}[P_j^{D}\|u_j\|+\Omega^{D}\|\varphi\|]\,dS, \tag{4}$$

where P_{ij}^{F} and Ω_i^{F}, are, respectively, the induced tractions and the electric displacement boundary value on the crack surfaces when a unit point force is applied in the ith direction; P_j^{D} and Ω^{D} are those corresponding to a unit point electric charge. In Eq. (4), $\|u_j\|$ and $\|\varphi\|$ denote, respectively, the elastic displacement and electric potential discontinuities across the crack face, defined as

$$\|u_i\|=u_i(S^+)-u_i(S^-),$$
$$\|\varphi\|=\varphi(S^+)-\varphi(S^-), \tag{5}$$

which are called the extended displacement discontinuities.

Inserting the extended point-force Green's functions [36] into Eq. (4) yields the following explicit expressions for the elastic displacement ($(u,\ v,\ w)=(u_1,\ u_2,\ u_3)\equiv(u_x,\ u_y,\ u_z)$) and electric potential

$$\begin{aligned}u=\int_{S^+}\Bigg\{&\Bigg[-2c_{66}D_4x\left(\frac{1}{R_4\tilde{R}_4^2}-\frac{2(\eta-y)^2}{R_4^2\tilde{R}_4^3}-\frac{(\eta-y)^2}{R_4^3\tilde{R}_4^2}\right)\\&-x\sum_{i=1}^{3}D_i\left(\frac{\xi_i}{R_i^3}-2c_{66}\left(\frac{3}{R_i\tilde{R}_i^2}-\frac{2x^2}{R_i^2\tilde{R}_i^3}-\frac{x^2}{R_i^3\tilde{R}_i^2}\right)\right)\Bigg]\|u\|\\&+c_{66}(\eta-y)\left[D_4\frac{1}{R_4^3}-\sum_{i=1}^{4}D_i\left(\frac{2}{R_i\tilde{R}_i^2}-\frac{4x^2}{R_i^2\tilde{R}_i^3}-\frac{2x^2}{R_i^3\tilde{R}_i^2}\right)\right]\|v\|\\&-D_4\left(\frac{1}{R_4\tilde{R}_4}-\frac{(\eta-y)^2}{R_4^3\tilde{R}_4}-\frac{(\eta-y)^2}{R_4^2\tilde{R}_4^2}\right)(\omega_{41}\|w\|+\omega_{42}\|\varphi\|)\\&+\sum_{i=1}^{3}D_i\left(\frac{1}{R_i\tilde{R}_i}-\frac{x^2}{R_i^3\tilde{R}_i}-\frac{x^2}{R_i^2\tilde{R}_i^2}\right)(\omega_{i1}\|w\|+\omega_{i2}\|\varphi\|)\Bigg\}dS(\eta,\varsigma),\end{aligned} \tag{6a}$$

$$\begin{aligned}v=\int_{S^+}\Bigg\{&\left[(\eta-y)\left(\sum_{i=1}^{3}D_i\frac{\xi_i}{R_i^3}+c_{66}\sum_{i=1}^{4}D_i\left(\frac{4x^2}{R_i^2\tilde{R}_i^3}+\frac{2x^2}{R_i^3\tilde{R}_i^2}-\frac{2}{R_i\tilde{R}_i^2}\right)\right)\right]\|u\|\\&-\left[c_{66}x\left(D_4\frac{1}{R_4^3}-\sum_{i=1}^{4}D_i\left(\frac{2}{R_i\tilde{R}_i^2}-\frac{4(\eta-y)^2}{R_i^2\tilde{R}_i^3}-\frac{2(\eta-y)^2}{R_i^3\tilde{R}_i^2}\right)\right)\right]\|v\|\\&+x(\eta-y)\sum_{i=1}^{4}D_i\left(\frac{1}{R_i^3\tilde{R}_i}+\frac{1}{R_i^2\tilde{R}_i^2}\right)(\omega_{i1}\|w\|+\omega_{i2}\|\varphi\|)\Bigg\}dS(\eta,\varsigma),\end{aligned} \tag{6b}$$

$$\begin{aligned}w=\int_{S^+}\Bigg\{&\left[2c_{66}\sum_{i=1}^{3}A_i\left(\frac{1}{R_i\tilde{R}_i}-\frac{x^2}{R_i^3\tilde{R}_i}-\frac{x^2}{R_i^2\tilde{R}_i^2}\right)+\sum_{i=1}^{3}\xi_iA_i\frac{(\varsigma_i-z_i)}{R_i^3}\right]\|u\|\\&+\left[2c_{66}x(\eta-y)\sum_{i=1}^{3}A_i\left(\frac{1}{R_i^3\tilde{R}_i}+\frac{1}{R_i{}^2\tilde{R}_i^2}\right)\right]\|v\|\\&-x\sum_{i=1}^{3}\frac{A_i}{R_i^3}(\omega_{i1}\|w\|+\omega_{i2}\|\varphi\|)\Bigg\}dS(\eta,\varsigma),\end{aligned} \tag{6c}$$

$$\begin{aligned}-\varphi=\int_{S^+}\Bigg\{&\left[2c_{66}\sum_{i=1}^{3}B_i\left(\frac{1}{R_i\tilde{R}_i}-\frac{x^2}{R_i^3\tilde{R}_i}-\frac{x^2}{R_i^2\tilde{R}_i^2}\right)+\sum_{i=1}^{3}\xi_iB_i\frac{(\varsigma_i-z_i)}{R_i^3}\right]\|u\|\\&+\left[2c_{66}x(\eta-y)\sum_{i=1}^{3}B_i\left(\frac{1}{R_i^3\tilde{R}_i}+\frac{1}{R_i{}^2\tilde{R}_i^2}\right)\right]\|v\|\\&-x\sum_{i=1}^{3}\frac{B_i}{R_i^3}(\omega_{i1}\|w\|+\omega_{i2}\|\varphi\|)\Bigg\}dS(\eta,\varsigma).\end{aligned} \tag{6d}$$

Eq. (6) indicates that the extended displacements at any internal point (x, y, z) can be expressed in terms of the extended displacement discontinuities across the surface of the vertical

crack, where

$$z_i = s_i z, \quad \varsigma_i = s_i \varsigma \quad (i=1,2,3,4),$$
$$R_i = \sqrt{x^2+(\eta-y)^2+(\varsigma_i-z_i)^2},$$
$$\tilde{R}_i = \sqrt{x^2+(\eta-y)^2+(\varsigma_i-z_i)^2}-(\varsigma_i-z_i), \tag{7}$$

and s_i are the roots of the material characteristic equation, while ω_{ij}, ξ_i, A_i, B_i and D_i are material-related constants given in [32]. It is noted that the constants D_i are different to the electric displacements defined in Eqs. (1) and (2).

4. Green's functions for extended displacement discontinuities

We assume that the vertical crack S is of a square shape with side length $2b=2d$ centered at the origin of the coordinate system, as shown in Fig. 2. First, when the size of the crack approaches zero, we then have the Green's functions or the fundamental solutions corresponding to a unit extended point displacement discontinuity. Therefore, these Green's functions should satisfy the governing equations of piezoelectric media subjected to the following conditions:

$$\lim_{b\to 0}\int_S \{\|u\|,\|v\|,\|w\|,\|\varphi\|\}\,dS = \{1,0,0,0\}, \tag{8a}$$

$$\lim_{b\to 0}\int_S \{\|u\|,\|v\|,\|w\|,\|\varphi\|\}\,dS = \{0,1,0,0\}, \tag{8b}$$

$$\lim_{b\to 0}\int_S \{\|u\|,\|v\|,\|w\|,\|\varphi\|\}\,dS = \{0,0,1,0\}, \tag{8c}$$

$$\lim_{b\to 0}\int_S \{\|u\|,\|v\|,\|w\|,\|\varphi\|\}\,dS = \{0,0,0,1\}. \tag{8d}$$

Making use of the method in deriving the extended point-displacement discontinuity Green's functions [35], we obtain the extended point-displacement discontinuity Green's functions satisfying Eqs. (8a)–(8d) for the case where a crack is vertical to the isotropic plane and parallel to the electric poling directions in a 3D transversely isotropic piezoelectric medium in Appendix A.

Now we assume that there is a rectangular element S_e of length $2b\times 2d$ in the *oyz* plane centered at the origin with its sides parallel to the axes of the coordinate system, as schematically shown in Fig. 2. The uniformly distributed extended displacement discontinuities $\|u^e\|$, $\|v^e\|$, $\|w^e\|$ and $\|\varphi^e\|$ are applied on the element. Integrating the extended point-displacement discontinuity Green's functions given in Appendix A on the element, we can obtain the extended Crouch fundamental solution due to the uniformly distributed extended displacement discontinuities as given in Appendix B.

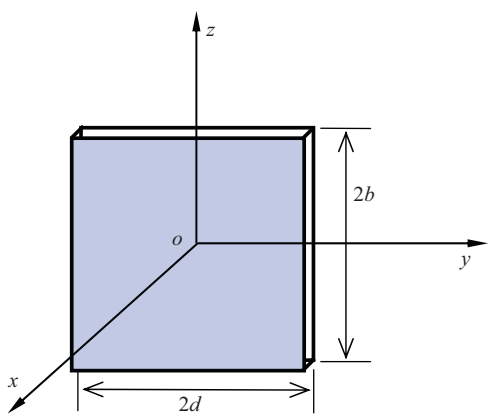

Fig. 2. A rectangular crack in the *oyz* plane centered at the origin of the coordinate system.

5. Extended displacement discontinuity boundary integral equations

Based on the Green's functions for unit extended point displacement discontinuities obtained in the previous section, the boundary integral equations of the vertical crack of arbitrary shape will be derived in this section and furthermore the nature of the singularity of the extended stresses along the crack front will be studied in the next section.

If the applied extended tractions on the crack faces satisfy

$$p_i|_{S^+} = -p_i|_{S^-}, \quad \omega|_{S^+} = -\omega|_{S^-}, \quad i=1,2,3 \text{ or } x,y,z, \tag{9}$$

and in the absence of the body force and electric charge, by using the Somigliana identity for a 3D piezoelectric medium [37] and the boundary conditions in Eq. (9), we obtain

$$p_i = \int_{S^+} (P_{ij}^{\|U\|}\|u_j\| + \Omega_i^{\|U\|}\|\varphi\|)\,dS,$$
$$\omega = \int_{S^+} (P_i^{\|\Phi\|}\|u_i\| + \Omega^{\|\Phi\|}\|\varphi\|)\,dS, \tag{10}$$

where (P_{ij}, Ω_i) and (U_{ij}, Φ_i) denotes, respectively, the extended traction and the extended displacement due to a unit extended point displacement discontinuity in the *i*th direction, and the superscripts $\|U\|$ and $\|\Phi\|$ denote the Green's functions corresponding to the displacement discontinuity and electric potential discontinuity, respectively.

Substituting the displacement discontinuity Green's functions obtained in the last section into Eq. (10), we obtain the extended displacement discontinuity boundary integral equations for an arbitrarily-shaped vertical crack

$$\int_{S^+}\Bigg\{4L_{11}^4\left[(\eta-y)^2\left(\frac{2}{r_4^2\tilde{r}_4^3}+\frac{1}{r_4^3\tilde{r}_4^2}\right)-\frac{1}{r_4\tilde{r}_4^2}\right]+\sum_{i=1}^{3}(6L_{12}^i+2L_{13}^i)\frac{1}{r_i\tilde{r}_i^2}$$
$$-\sum_{i=1}^{3}2L_{13}^i(\eta-y)^2\left(\frac{2}{r_i^2\tilde{r}_i^3}+\frac{1}{r_i^3\tilde{r}_i^2}\right)-\sum_{i=1}^{3}(L_{14}^i+L_{15}^i+2L_{16}^i+L_{17}^i)\frac{1}{r_i^3}$$
$$+\sum_{i=1}^{3}3L_{15}^i\frac{(\eta-y)^2}{r_i^5}+\sum_{i=1}^{3}3L_{17}^i\frac{(\varsigma_i-z_i)^2}{r_i^5}\Bigg\}\|u\|\,dS=-p_x(y,z), \tag{11a}$$

$$\int_{S^+}\Bigg\{\Bigg[L_{11}^4\left(\frac{4}{r_4\tilde{r}_4^2}-\frac{2}{r_4^3}-(\eta-y)^2\left(-\frac{3}{r_4^5}+\frac{8}{r_4^2\tilde{r}_4^3}+\frac{4}{r_4^3\tilde{r}_4^2}\right)\right)$$
$$+4\sum_{i=1}^{3}L_{11}^i\left(\frac{1}{r_i\tilde{r}_i^2}-(\eta-y)^2\left(\frac{2}{r_i^2\tilde{r}_i^3}+\frac{1}{r_i^3\tilde{r}_i^2}\right)\right)\Bigg]\|v\|$$
$$+\left(\frac{6(\eta-y)}{r_4^2\tilde{r}_4^2}-(\eta-y)^3\left(\frac{3}{r_4^5\tilde{r}_4}+\frac{3}{r_4^4\tilde{r}_4^2}+\frac{4}{r_4^3\tilde{r}_4^3}\right)\right)\left(L_{31}^4\|w\|+L_{32}^4\|\varphi\|\right)$$
$$-\sum_{i=1}^{3}2(\eta-y)\left(\frac{1}{r_i^2\tilde{r}_i^2}+\frac{1}{r_i^3\tilde{r}_i}\right)(L_{34}^i\|w\|+L_{35}^i\|\varphi\|)\Bigg\}dS=-p_y(y,z), \tag{11b}$$

$$\int_{S^+}\Bigg\{\Bigg[\left(2(\eta-y)\left(\frac{1}{r_4^2\tilde{r}_4^2}+\frac{1}{r_4^3\tilde{r}_4}\right)-(\eta-y)^3\left(\frac{2}{r_4^3\tilde{r}_4^3}+\frac{3}{r_4^4\tilde{r}_4^2}+\frac{3}{r_4^5\tilde{r}_4}\right)\right)L_{21}^4$$
$$-\sum_{i=1}^{3}2(\eta-y)\left(\frac{1}{r_i^2\tilde{r}_i^2}+\frac{1}{r_i^3\tilde{r}_i}\right)L_{21}^i\Bigg]\|v\|$$
$$+\left[\frac{1}{r_4^3}-3\frac{(\eta-y)^2}{r_4^5}\right](L_{41}^4\|w\|+L_{61}^4\|\varphi\|)$$
$$-\sum_{i=1}^{3}\frac{1}{r_i^3}(L_{51}^i\|w\|+L_{71}^i\|\varphi\|)\Bigg\}dS=-p_z(y,z), \tag{11c}$$

$$\int_{S^+}\left\{\left[\left(2(\eta-y)\left(\frac{1}{r_4^2\tilde{r}_4^2}+\frac{1}{r_4^3\tilde{r}_4}\right)-(\eta-y)^3\left(\frac{2}{r_4^3\tilde{r}_4^3}+\frac{3}{r_4^4\tilde{r}_4^2}+\frac{3}{r_4^5\tilde{r}_4}\right)\right)L_{22}^4 -\sum_{i=1}^{3}2(\eta-y)\left(\frac{1}{r_i^2\tilde{r}_i^2}+\frac{1}{r_i^3\tilde{r}_i}\right)L_{22}^i\right]\|v\| +\left[\frac{1}{r_4^3}-3\frac{(\eta-y)^2}{r_4^5}\right](L_{42}^4\|w\|+L_{62}^4\|\varphi\|) -\sum_{i=1}^{3}\frac{1}{r_i^3}(L_{52}^i\|w\|+L_{72}^i\|\varphi\|)\right\}dS=-\omega(y,z), \tag{11d}$$

where

$$r_i=\sqrt{(\eta-y)^2+(\varsigma_i-z_i)^2},$$
$$\tilde{r}_i=\sqrt{(\eta-y)^2+(\varsigma_i-z_i)^2}+(\varsigma_i-z_i)\quad(i=1,2,3,4), \tag{12}$$

and the material-related constants L_{kl}^i are given by

$$L_{11}^4=D_4c_{66}c_{66},\quad L_{12}^i=D_ic_{66}c_{11},\quad L_{13}^i=D_ic_{66}c_{12},$$
$$L_{14}^i=D_i\xi_ic_{11},\quad L_{15}^i=D_i\xi_ic_{12},\quad L_{16}^i=(A_ic_{13}-B_ie_{31})c_{66}s_i,$$
$$L_{17}^i=(A_ic_{13}-B_ie_{31})\xi_is_i,\quad L_{2j}^i=D_i\omega_{ij}c_{66},$$
$$L_{31}^4=D_4c_{66}c_{44}s_4,\quad L_{34}^i=c_{66}(c_{44}D_is_i+c_{44}A_i-e_{15}B_i),$$
$$L_{4i}^4=D_4c_{44}\omega_{4i}s_4,\quad L_{5j}^i=\omega_{ij}(c_{44}D_is_i+c_{44}A_i-e_{15}B_i),$$
$$L_{32}^4=D_4c_{66}e_{15}s_4,\quad L_{35}^i=c_{66}(e_{15}D_is_i+e_{15}A_i+\varepsilon_{11}B_i),$$
$$L_{6i}^4=D_4e_{15}\omega_{4i}s_4,\quad L_{7j}^i=\omega_{ij}(e_{15}D_is_i+e_{15}A_i+\varepsilon_{11}B_i). \tag{13}$$

Of particular interesting is the fact that the displacement discontinuity in the normal direction $\|u\|$ appears only in Eq. (11a). In other words, it is decoupled from the other extended displacement discontinuities and dependent only on the normal traction p_x. On the other hand, the other three extended displacement discontinuities $\|v\|$, $\|w\|$ and $\|\varphi\|$ are clearly coupled in Eqs. (11b)–(11d). This feature is fundamentally different to that associated with a horizontal crack (or a crack in the isotropic plane [6,22]) where the displacement discontinuities $\|u\|$ and $\|v\|$ on the crack faces are coupled, and the displacement discontinuity $\|w\|$ and the electric potential discontinuity $\|\varphi\|$ are coupled. As such, it is important to investigate the fracture mechanics of the vertical crack in a transversely isotropic piezoelectric solid.

6. Singular behavior and field intensity factors

Knowing the singular behavior of fields near the crack tip and calculating the field intensity factors are the key tasks in fracture mechanics. Due to the complexity of the three-dimensional problem, only the singular behaviors near some special points are investigated in the present paper.

Consider the special point on the smooth portion of the crack front Γ where z reaches the minimum value, we place a Cartesian coordinate system $oxyz$ such that the y-axis and z-axis are, respectively, tangential and normal to Γ, while the x-axis is normal to the crack plane S, as depicted in Fig. 3a.

We define the infinitesimal ε as the radius of a circle $\sum$ centered at point o on crack S as shown in Fig. 3a. Based on the elastic fracture theory [38], the extended displacement near the crack tip o can be obtained by superposing the extended in-plane and anti-plane displacements. Therefore, at the neighborhood of point o, the extended displacement discontinuities can be expressed asymptotically as

$$\|u\|=A_x(o)\varsigma^{\alpha_x},\quad \|v\|=A_y(o)\varsigma^{\alpha_y},\quad \|w\|=A_z(o)\varsigma^{\alpha_z},\quad \|\varphi\|=A_\varphi(o)\varsigma^{\alpha_\varphi}, \tag{14}$$

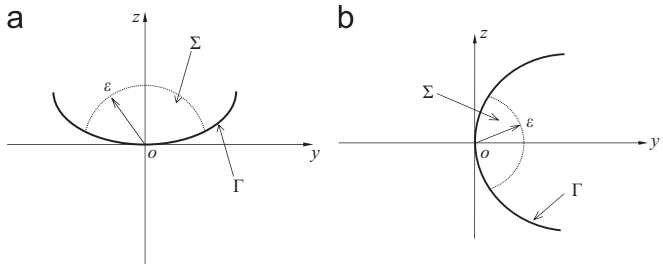

Fig. 3. (a) Local coordinate system at the crack tip of its lower front of the vertical crack in the *oyz* plane of the *oxyz* system. (b) Local coordinate system at the crack tip of its left front of the vertical crack in the *oyz* plane of the *oxyz* system.

where A_x, A_y, A_z, A_φ are coefficients to be evaluated at the origin o, and α_x, α_y, α_z, α_φ are the so-called singular indices of the extended displacements with values lying between (0,1).

Substituting Eq. (14) into Eq. (11), letting ε be sufficiently small and taking the limit $z\to 0$, and further making use of the finite-part integral theory, we obtain the conditions for the existence of a non-trivial solution

$$\cot\pi\alpha_x=\cot\pi\alpha_y=\cot\pi\alpha_z=\cot\pi\alpha_\varphi=0. \tag{15}$$

Therefore, we obtain the singular indices

$$\alpha_x=\alpha_y=\alpha_z=\alpha_\phi=1/2. \tag{16}$$

Eq. (16) indicates that near the crack front, the field behaves the same way as in the classical fracture mechanics with singularity $O(1/\sqrt{r})$, which is further identical to the singularity when the crack is along the isotropy plane [6,22].

Substituting Eq. (16) into Eq. (14), and using Eq. (10), we obtain the following extended stress components at point $(0,0,-\rho)$:

$$\sigma_{xx}=k_{11}A_x(o)\pi/\sqrt{\rho},$$
$$\sigma_{xy}=-k_{12}A_y(o)\pi/\sqrt{\rho},$$
$$\sigma_{xz}=-\sum_{i=1}^{3}[L_{51}^iA_z(o)+L_{71}^iA_\varphi(o)]\frac{1}{s_i^2}\pi/\sqrt{\rho},$$
$$D_x=-\sum_{i=1}^{3}[L_{52}^iA_z(o)+L_{72}^iA_\varphi(o)]\frac{1}{s_i^2}\pi/\sqrt{\rho}, \tag{17}$$

where

$$k_{11}=\sum_{i=1}^{3}\frac{1}{s_i^2}(2L_{12}^i-L_{14}^i-2L_{16}^i+L_{17}^i),$$
$$k_{12}=L_{11}^4\frac{1}{s_4^2}. \tag{18}$$

Substituting Eqs. (17) and (14) into the definition of the field intensity factors

$$K_{\mathrm{I}}^{\mathrm{F}}=\lim_{\rho\to 0}\sqrt{2\pi\rho}\sigma_{xx}(0,0,-\rho),$$
$$K_{\mathrm{I}}^{\mathrm{D}}=\lim_{\rho\to 0}\sqrt{2\pi\rho}D_x(0,0,-\rho),$$
$$K_{\mathrm{II}}^{\mathrm{F}}=\lim_{\rho\to 0}\sqrt{2\pi\rho}\sigma_{xz}(0,0,-\rho),$$
$$K_{\mathrm{III}}^{\mathrm{F}}=\lim_{\rho\to 0}\sqrt{2\pi\rho}\sigma_{xy}(0,0,-\rho), \tag{19}$$

the extended field intensity factor at a crack tip along the horizontal front of the vertical crack can be finally expressed in terms of the extended displacement discontinuities as

$$K_{\mathrm{I}}^{\mathrm{F}}=\sqrt{2\pi}\pi\lim_{z\to 0}k_{11}\|u\|/\sqrt{z},$$

$$K_{\mathrm{I}}^{\mathrm{D}}=-\sqrt{2\pi}\pi\lim_{z\to 0}\sum_{i=1}^{3}[L_{52}^i\|w\|+L_{72}^i\|\varphi\|]\frac{1}{s_i^2}/\sqrt{z},$$

$$K_{\mathrm{II}}^{\mathrm{F}} = -\sqrt{2\pi}\pi \lim_{z\to 0} \sum_{i=1}^{3} [L_{51}^{i} \|w\| + L_{71}^{i} \|\varphi\|] \frac{1}{s_i^2} / \sqrt{z},$$
$$K_{\mathrm{III}}^{\mathrm{F}} = -\sqrt{2\pi}\pi \lim_{z\to 0} k_{12} \|v\| / \sqrt{z}. \tag{20}$$

Similarly, for a crack tip along the left front of the vertical crack as schematically shown in Fig. 3b, the extended field intensity factors in terms of the extended displacement discontinuities can be found as

$$K_{\mathrm{I}}^{\mathrm{F}} = \sqrt{2\pi}\pi \lim_{y\to 0} k_{21} \|u\| / \sqrt{y},$$
$$K_{\mathrm{I}}^{\mathrm{D}} = -\sqrt{2\pi}\pi \lim_{y\to 0} [k_{63} \|v\| + k_{53} \|w\| + k_{33} \|\varphi\|] / \sqrt{y},$$
$$K_{\mathrm{II}}^{\mathrm{F}} = -\sqrt{2\pi}\pi \lim_{y\to 0} [k_{61} \|v\| + k_{51} \|w\| + k_{31} \|\varphi\|] / \sqrt{y},$$
$$K_{\mathrm{III}}^{\mathrm{F}} = -\sqrt{2\pi}\pi \lim_{y\to 0} [k_{62} \|v\| + k_{52} \|w\| + k_{32} \|\varphi\|] / \sqrt{y}, \tag{21}$$

where the material-related constants are given by

$$k_{21} = \frac{2}{s_4} L_{11}^{4} + \sum_{i=1}^{3} [3L_{12}^{i} - L_{13}^{i} - L_{14}^{i} + L_{15}^{i} - 2L_{16}^{i}] \frac{1}{s_i},$$
$$k_{31} = \frac{1}{s_4} L_{32}^{4} + \sum_{i=1}^{3} \frac{2}{s_i} L_{35}^{i}, \quad k_{32} = \frac{1}{s_4} L_{61}^{4} + \sum_{i=1}^{3} \frac{1}{s_i} L_{71}^{i},$$
$$k_{33} = \frac{1}{s_4} L_{62}^{4} + \sum_{i=1}^{3} \frac{1}{s_i} L_{72}^{i}, \quad k_{51} = \frac{1}{s_4} L_{31}^{4} + \sum_{i=1}^{3} \frac{2}{s_i} L_{34}^{i},$$
$$k_{52} = \frac{1}{s_4} L_{41}^{4} + \sum_{i=1}^{3} \frac{1}{s_i} L_{51}^{i}, \quad k_{53} = \frac{1}{s_4} L_{42}^{4} + \sum_{i=1}^{3} \frac{1}{s_i} L_{52}^{i},$$
$$k_{61} = \frac{2}{s_4} L_{11}^{4} + \sum_{i=1}^{3} \frac{2}{s_i} L_{11}^{i}, \quad k_{62} = \frac{1}{s_4} L_{21}^{4} + \sum_{i=1}^{3} \frac{2}{s_i} L_{21}^{i},$$
$$k_{63} = \frac{1}{s_4} L_{22}^{4} + \sum_{i=1}^{3} \frac{2}{s_i} L_{22}^{i}. \tag{22}$$

Eqs. (20) and (21) show that for a vertical crack, the mode I stress intensity factor $K_{\mathrm{I}}^{\mathrm{F}}$ is only related to the normal displacement discontinuity $\|u\|$. It is further observed that, for the vertical crack case, the electric displacement intensity factor $K_{\mathrm{I}}^{\mathrm{D}}$ and the mode II stress intensity factor $K_{\mathrm{II}}^{\mathrm{F}}$ at the crack tip of the vertical crack front depend on the displacement discontinuities $\|w\|$ and $\|\varphi\|$, as well as on $\|v\|$. These features again demonstrates that the relations between the extended field intensity factors and the extended displacement discontinuities for a vertical crack are remarkably different to the situation where cracks are located in the plane of isotropy of the piezoelectric media [6,22].

7. Extended displacement discontinuity boundary element method

Following Zhao et al. [35], an extended displacement discontinuity boundary element approach is adapted to numerically analyze the vertical crack behaviors in transversely isotropic piezoelectric 3D media.

If the uniformly distributed extended displacement discontinuities $\|u^{\mathrm{e}}\|$, $\|v^{\mathrm{e}}\|$, $\|w^{\mathrm{e}}\|$ and $\|\varphi^{\mathrm{e}}\|$ are applied on the element or a rectangular element S_{e} in the *oyz* plane, as schematically shown in Fig. 2, the extended stress fields are given in Eq. (B1), which can be rewritten in the following compact form:

$$\sigma_i^{\mathrm{e}} = \sum_{j=1}^{4} T_{ij}^{\mathrm{e}} \|u_j^{\mathrm{e}}\|, \quad i,j = 1-4 \tag{23}$$

where T_{ij}^{e} are the Green's functions or the extended Crouch fundamental solutions of the rectangular element, and $\sigma_1^{\mathrm{e}} = \sigma_{xx}^{\mathrm{e}}$, $\sigma_2^{\mathrm{e}} = \sigma_{xy}^{\mathrm{e}}$, $\sigma_3^{\mathrm{e}} = \sigma_{xz}^{\mathrm{e}}$, $\sigma_4^{\mathrm{e}} = D_x^{\mathrm{e}}$, $u_1^{\mathrm{e}} = u^{\mathrm{e}}$, $u_2^{\mathrm{e}} = v^{\mathrm{e}}$, $u_3^{\mathrm{e}} = w^{\mathrm{e}}$, $u_4^{\mathrm{e}} = \varphi^{\mathrm{e}}$.

The domain of the crack is divided into N square elements. The geometric centroid of the eth element is denoted by (y_e, z_e). From the extended Crouch fundamental solution, the extended stresses at the centroid of element q can be obtained by superposing the contribution of all elements. Using the boundary conditions on the crack faces, one obtain

$$\sum_{e=1}^{N} \sum_{j=1}^{4} T_{ij}^{\mathrm{e}}(y_q - y_e, z_q - z_e) \|u_i^{\mathrm{e}}\| = \sigma_i^0(q), \quad q = 1,2,\ldots,N, \tag{24}$$

where σ_i^0 are the applied extended loadings on the crack face.

Solving Eq. (24), we obtain the extended displacement discontinuities on the crack faces. With these, the extended field intensity factors can be calculated by using Eqs. (20) and (21).

8. Numerical results and discussion

We consider a square crack of side length $2a$ in an infinite piezoelectric medium in the *oyz* plane. The material is $BaTiO_3$ with the following coefficients:

$$c_{11} = 16.6 \times 10^{10}\,\mathrm{N\,m^{-2}}, \quad c_{12} = 7.7 \times 10^{10}\,\mathrm{N\,m^{-2}}, \quad c_{13} = 7.8 \times 10^{10}\,\mathrm{N\,m^{-2}},$$
$$c_{33} = 16.2 \times 10^{10}\,\mathrm{N\,m^{-2}}, \quad c_{44} = 4.3 \times 10^{10}\,\mathrm{N\,m^{-2}},$$
$$e_{31} = -4.4\,\mathrm{C\,m^{-2}}, \quad e_{33} = 18.6\,\mathrm{C\,m^{-2}}, \quad e_{15} = 11.6\,\mathrm{C\,m^{-2}},$$
$$\kappa_{11} = 112 \times 10^{-10}\,\mathrm{C(V\,m)^{-1}}, \quad \kappa_{33} = 126 \times 10^{-10}\,\mathrm{C(V\,m)^{-1}}. \tag{25}$$

Fig. 4 shows the variation of the elastic displacement discontinuity $\|u\|$ at the crack center as a function of the uniform loading P_x applied to the crack surface, whilst Fig. 5 displays the variation of the extended displacement discontinuities $\|v\|$, $\|w\|$ and $\|\varphi\|$ at the crack center vs. the uniform surface loading D_x. The results show that there is only elastic displacement discontinuity $\|u\|$ under pure mechanical loading, whilst the extended displacement discontinuities $\|v\|$, $\|w\|$ and $\|\varphi\|$ exist at the crack center under the uniform electric loading D_x. These results also demonstrate the special coupling behavior of the extended displacement discontinuities in the boundary integral equations (11). In both cases, other loads on the crack surface are assumed to be zero. These results are calculated by the extended displacement discontinuity method using $N = 15 \times 15$ elements. It is observed from these two figures that with only 225 constant elements, very accurate results can be obtained as compared to the results using the finite element software ANSYS (Figs. 4 and 5).

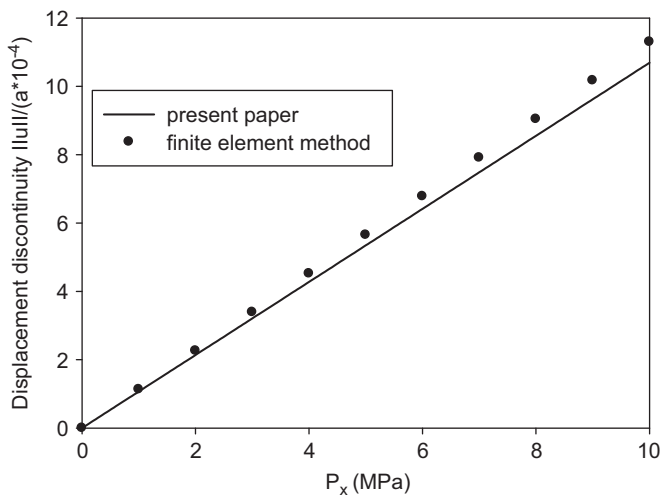

Fig. 4. Variation of the displacement discontinuity $\|u\|$ at the center of the square crack with the applied mechanical load P_x on the crack surface (other loads on the crack surface are zero): present paper (via the extended displacement discontinuity boundary element method) vs. finite element method.

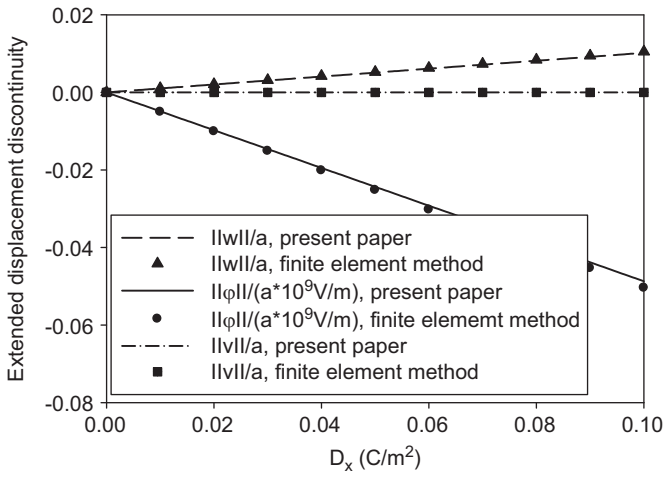

Fig. 5. Variation of the extended displacement discontinuities $\|v\|$, $\|w\|$ and $\|\varphi\|$ at the center of the square crack with the applied electric load D_x on the crack surface (other loads on the crack surface are zero): present paper (via the extended displacement discontinuity boundary element method) vs. finite element method.

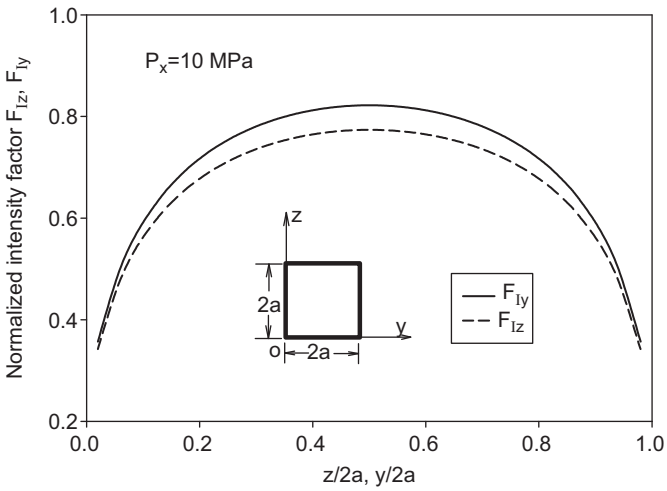

Fig. 6. Variation of the normalized mode I stress intensity factors along the crack front parallel to z-axis (F_{Iz}) and y-axis (F_{Iy}), under the mechanical load $P_x=10$ MPa on the crack surface (other loads on the crack surface are zero).

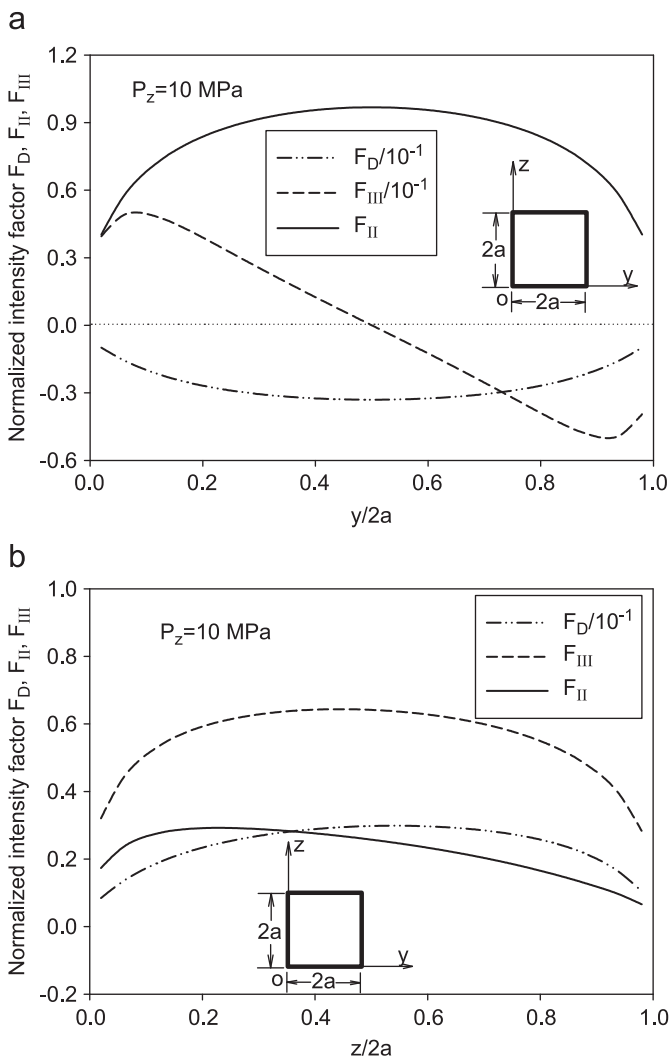

Fig. 7. (a) Variation of the normalized extended field intensity factors along the crack front parallel to y-axis, under the mechanical load $P_z=10$ MPa on the crack surface (other loads on the crack surface are zero). (b) Variation of the normalized extended field intensity factors along the crack front parallel to z-axis, under the mechanical load $P_z=10$ MPa on the crack surface (other loads on the crack surface are zero).

Fig. 6 shows the normalized mode I stress intensity factor F_I along the crack front due to the uniform force P_x applied on the crack surface

$$F_I = \frac{K_I}{P_x\sqrt{\pi a}}, \tag{26}$$

along the crack front, where the subscripts "z" and "y" denote, respectively, the crack front parallel to the z- and y-axis. It is observed that, under this mechanical loading, the only nonzero intensity factor along the crack fronts is F_I, which is symmetrical with respect to the midpoint of each side and reaches its maximum value at the midpoint. Since the poling direction is along the z-axis and vertical to y-axis, the stress intensity factor along the crack front parallel to the y-axis is larger than that along the crack front parallel to the z-axis.

Fig. 7a and b plot the nonzero extended normalized field intensity factors F_D, F_{II} and F_{III} along the crack front parallel to the y- and z-axis, respectively. The uniform shear load on the crack surface is $P_z=10$ MPa while other loads are assumed to be zero. The extended field intensity factors are normalized by

$$F_D = \frac{K_D}{\chi P_z\sqrt{\pi a}}, \quad F_{II} = \frac{K_{II}}{P_z\sqrt{\pi a}}, \quad F_{III} = \frac{K_{III}}{P_z\sqrt{\pi a}}, \tag{27}$$

where $\chi=\kappa_{33}/e_{33}$. Fig. 7a demonstrates that the extended normalized field intensity factors F_D and F_{II} along the crack front parallel to the y-axis are symmetrical, and F_{III} is anti-symmetrical, with respect to the middle point of the crack front. However, due to the effect of the poling direction, these symmetric properties disappear along the crack front parallel to the z-axis as shown in Fig. 7b.

Fig. 8a and b show the nonzero extended normalized field intensity factors F_D, F_{II} and F_{III} along the crack fronts under the mechanical shear loading $P_y=10$ MPa while other loads are zero. Similarly, the normalized field intensity factors are defined by

$$F_D = \frac{K_D}{\chi P_y\sqrt{\pi a}}, \quad F_{II} = \frac{K_{II}}{P_y\sqrt{\pi a}}, \quad F_{III} = \frac{K_{III}}{P_y\sqrt{\pi a}}. \tag{28}$$

It is noticed from Fig. 8a that, along the crack front parallel to the y-axis, F_{III} is symmetrical, whilst F_D and F_{II} are anti-symmetric.

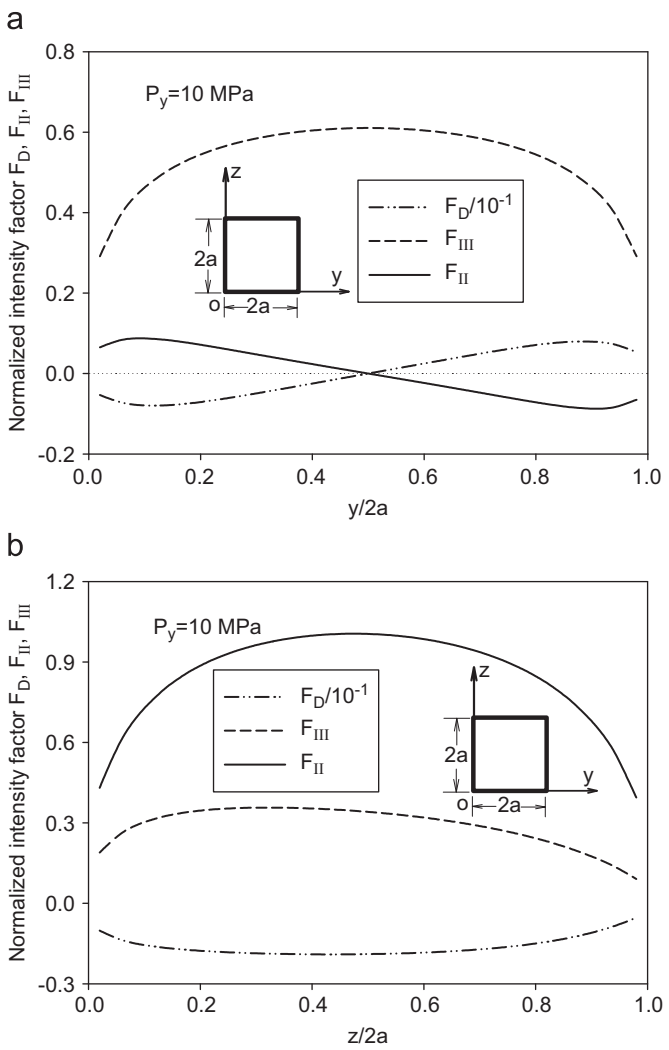

Fig. 8. (a) Variation of the normalized extended field intensity factors along the crack front parallel to y-axis, under the mechanical load P_y=10 MPa on the crack surface (other loads on the crack surface are zero). (b) Variation of the normalized extended field intensity factors along the crack front parallel to z-axis, under the mechanical load P_y=10 MPa on the crack surface (other loads on the crack surface are zero).

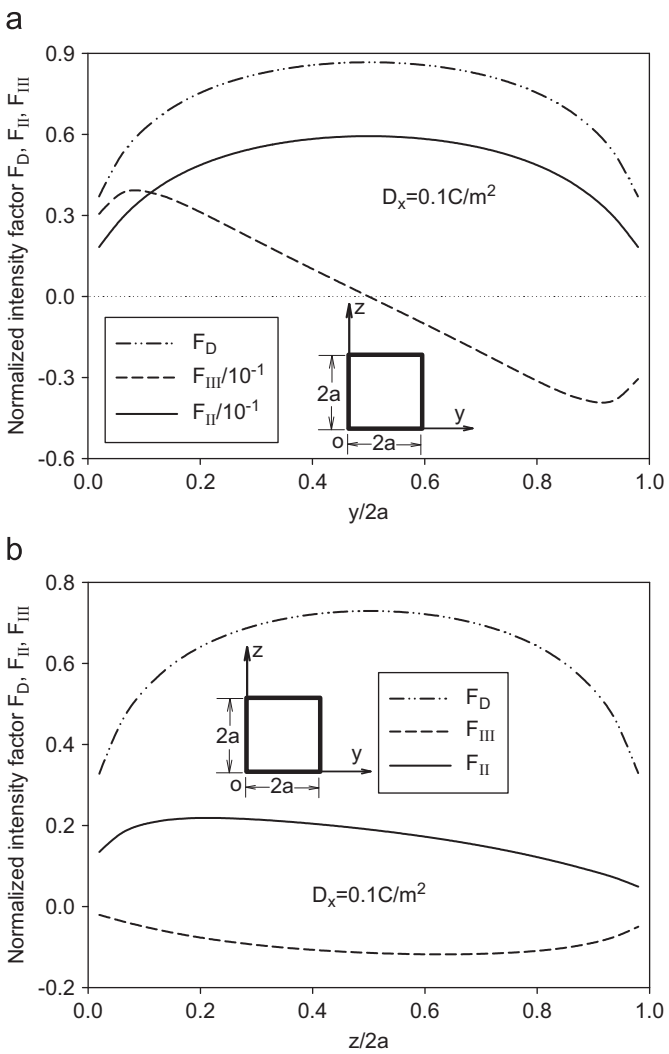

Fig. 9. (a) Variation of the normalized extended field intensity factors along the crack front parallel to y-axis, under the electric load D_x=0.1 C m^{-2} on the crack surface (other loads on the crack surface are zero). (b) Variation of the normalized extended field intensity factors along the crack front parallel to z-axis, under the electric load D_x=0.1 C m^{-2} on the crack surface (other loads on the crack surface are zero).

On the other hand, along the crack front parallel to the z-axis, these extended field intensity factors posses no symmetric feature (Fig. 8b) due to the poling direction selected.

Fig. 9a and b plot the nonzero extended normalized field intensity factors F_D, F_{II} and F_{III} along the crack fronts under the electric loading D_x=0.1 C m^{-2} with the mechanical loads being zero. These intensity factors are normalized by

$$F_D = \frac{K_D}{D_x\sqrt{\pi a}}, \quad F_{II} = \frac{\chi K_{II}}{D_x\sqrt{\pi a}}, \quad F_{III} = \frac{\chi K_{III}}{D_x\sqrt{\pi a}}. \tag{29}$$

It is observed that while along the crack front parallel to the y-axis, these intensity factors exhibit either symmetric or anti-symmetric behaviors (Fig. 9a), those along the crack front parallel to the z-axis are not symmetric due to the poling direction chosen (Fig. 9b).

9. Concluding remarks

The conventional displacement discontinuity method has been extended to analyze vertical cracks in transversely isotropic piezoelectric 3D media. The Green's functions or extended Crouch fundamental solutions corresponding to the extended elastic displacement discontinuities have been derived by making use of the fundamental solutions of an extended point force and the Somigliana identity. The hyper-singular displacement discontinuity boundary integral equations and the extended field intensity factors in terms of the extended displacement discontinuities on the crack faces have been derived. For the special crack orientation studied in this paper, the following conclusions can be drawn:

(1) Special coupling behavior has been found in the boundary integral equations: the normal displacement discontinuity $\|u\|$ is decoupled from the other extended displacement discontinuities, which is fundamentally different from that for the crack in the isotropic plane.
(2) The singularity index near the vertical crack tip is still 1/2. However, the expressions of the extended stress intensity factor show the anisotropic property.
(3) The mode I stress intensity factor K_I^F is related only to the displacement discontinuity or the mechanical loading in the direction normal to the crack plane, whilst the other field

intensity factors are coupled together, with their features depending on the crack tip location and the poling direction.

The displacement discontinuity method has been coded to calculate the extended displacement discontinuities on the crack surface and the field intensity factors along the crack fronts. The program has been validated by the commercial code ANSYS. Numerical results have demonstrated further that the poling direction (with respect to the crack surface) can significantly influence the fracture mechanics behavior of the cracks in piezoelectric 3D media.

Acknowledgment

The work was supported by the National Natural Science Foundation of China (Nos. 11102186, 11072221 and 10872184), the Program for Innovative Research Team (in Science and Technology) in University of Henan Province (2010IRTSTHN013) and the Bairen Program in Henan Province.

Appendix A. Green's functions for extended unit point displacement discontinuities

A.1. Green's function satisfying Eq. (8a)

$$u=-2c_{66}D_4x\left(\frac{1}{R_4\tilde{R}_4^2}-\frac{2y^2}{R_4^2\tilde{R}_4^3}-\frac{y^2}{R_4^3\tilde{R}_4^2}\right)-x\sum_{i=1}^{3}D_i\left(\frac{\xi_i}{R_i^3}-2c_{66}\left(\frac{3}{R_i\tilde{R}_i^2}-\frac{2x^2}{R_i^2\tilde{R}_i^3}-\frac{x^2}{R_i^3\tilde{R}_i^2}\right)\right), \tag{A1a}$$

$$v=-y\left(\sum_{i=1}^{3}D_i\frac{\xi_i}{R_i^3}+c_{66}\sum_{i=1}^{4}D_i\left(\frac{4x^2}{R_i^2\tilde{R}_i^3}+\frac{2x^2}{R_i^3\tilde{R}_i^2}-\frac{2}{R_i\tilde{R}_i^2}\right)\right), \tag{A1b}$$

$$w=2c_{66}\sum_{i=1}^{3}A_i\left(\frac{1}{R_i\tilde{R}_i}-\frac{x^2}{R_i^3\tilde{R}_i}-\frac{x^2}{R_i^2\tilde{R}_i^2}\right)-\sum_{i=1}^{3}\xi_iA_i\frac{z_i}{R_i^3}, \tag{A1c}$$

$$\varphi=-2c_{66}\sum_{i=1}^{3}B_i\left(\frac{1}{R_i\tilde{R}_i}-\frac{x^2}{R_i^3\tilde{R}_i}-\frac{x^2}{R_i^2\tilde{R}_i^2}\right)+\sum_{i=1}^{3}\xi_iB_i\frac{z_i}{R_i^3}, \tag{A1d}$$

where

$$R_i=\sqrt{x^2+y^2+z_i^2},$$
$$\tilde{R}_i=\sqrt{x^2+y^2+z_i^2}+z_i \quad (i=1,2,3,4). \tag{A2}$$

A.2. Green's function satisfying Eq. (8b)

$$u=-c_{66}y\left[D_4\frac{1}{R_4^3}-\sum_{i=1}^{4}D_i\left(\frac{2}{R_i\tilde{R}_i^2}-\frac{4x^2}{R_i^2\tilde{R}_i^3}-\frac{2x^2}{R_i^3\tilde{R}_i^2}\right)\right], \tag{A3a}$$

$$v=c_{66}x\left[D_4\frac{1}{R_4^3}-\sum_{i=1}^{4}D_i\left(\frac{2}{R_i\tilde{R}_i^2}-\frac{4y^2}{R_i^2\tilde{R}_i^3}-\frac{2y^2}{R_i^3\tilde{R}_i^2}\right)\right], \tag{A3b}$$

$$w=-2c_{66}xy\sum_{i=1}^{3}A_i\left(\frac{1}{R_i^3\tilde{R}_i}+\frac{1}{R_i{}^2\tilde{R}_i^2}\right), \tag{A3c}$$

$$\varphi=2c_{66}xy\sum_{i=1}^{3}B_i\left(\frac{1}{R_i^3\tilde{R}_i}+\frac{1}{R_i{}^2\tilde{R}_i^2}\right). \tag{A3d}$$

A.3. Green's function satisfying Eq. (8c)

$$u=-\omega_{41}D_4\left(\frac{1}{R_4\tilde{R}_4}-\frac{y^2}{R_4^3\tilde{R}_4}-\frac{y^2}{R_4^2\tilde{R}_4^2}\right)+\sum_{i=1}^{3}\omega_{i1}D_i\left(\frac{1}{R_i\tilde{R}_i}-\frac{x^2}{R_i^3\tilde{R}_i}-\frac{x^2}{R_i^2\tilde{R}_5^2}\right), \tag{A4a}$$

$$v=-\sum_{i=1}^{4}\omega_{i1}D_ixy\left(\frac{1}{R_i^3\tilde{R}_i}+\frac{1}{R_i^2\tilde{R}_i^2}\right), \tag{A4b}$$

$$w=-x\sum_{i=1}^{3}\frac{\omega_{i1}A_i}{R_i^3}, \tag{A4c}$$

$$\varphi=x\sum_{i=1}^{3}\frac{\omega_{i1}B_i}{R_i^3}. \tag{A4d}$$

A.4. Green's function satisfying Eq. (8d)

The Green's functions satisfying Eq. (8d) can be obtained from Eq. (A4) by simply replacing ω_{i1} by ω_{i2}.

Substituting the obtained extended displacements into the constitutive equations (2), the extended stress can be obtained.

Appendix B. Extended Crouch fundamental solutions

When the uniformly distributed extended displacement discontinuities $\|u^e\|$, $\|v^e\|$, $\|w^e\|$ and $\|\varphi^e\|$ are applied on a rectangular element S_e of length $2b\times 2d$ in the oyz plane, as schematically shown in Fig. 2, the extended Crouch fundamental solution can be expressed as

$$\sigma_{xx}^e=\left[4L_{11}^4Q_1^4+\sum_{i=1}^{3}((6L_{12}^i+2L_{13}^i)Q_2^i-2L_{13}^iQ_3^i-(L_{14}^i+L_{15}^i+2L_{16}^i)Q_4^i+3L_{15}^iQ_5^i+L_{17}^iQ_6^i)\right]\|u^e\|, \tag{B1a}$$

$$\sigma_{xy}^e=\left[L_{11}^4(-4Q_1^4+3Q_5^4-2Q_4^4)-4\sum_{i=1}^{3}L_{11}^iQ_1^i\right]\|v^e\|+\left[L_{21}^4(2Q_7^4-Q_8^4)-2\sum_{i=1}^{3}L_{21}^iQ_7^i\right]\|w^e\|+\left[L_{22}^4(2Q_7^4-Q_8^4)-2\sum_{i=1}^{3}L_{22}^iQ_7^i\right]\|\varphi^e\|, \tag{B1b}$$

$$\sigma_{xz}^e=\left[L_{31}^4Q_9^4-\sum_{i=1}^{3}2L_{34}^iQ_7^i\right]\|v^e\|+\left[L_{41}^4(Q_4^4-3Q_5^4)-\sum_{i=1}^{3}L_{51}^iQ_4^i\right]\|w^e\|+\left[L_{42}^4(Q_4^4-3Q_5^4)-\sum_{i=1}^{3}L_{52}^iQ_4^i\right]\|\varphi^e\|, \tag{B1c}$$

$$D_x^e=\left[L_{32}^4Q_9^4-\sum_{i=1}^{3}2L_{35}^iQ_7^i\right]\|v^e\|+\left[L_{61}^4(Q_4^4-3Q_5^4)-\sum_{i=1}^{3}L_{71}^iQ_4^i\right]\|w^e\|+\left[L_{62}^4(Q_4^4-3Q_5^4)-\sum_{i=1}^{3}L_{72}^iQ_4^i\right]\|\varphi^e\|, \tag{B1d}$$

where the functions are given by

$$Q_1^i=F_{11}^i+F_{12}^i+M_{11}^iG_{11}^i+M_{12}^iG_{12}^i-M_{13}^iG_{13}^i-M_{14}^iG_{14}^i,$$
$$Q_2^i=-(M_{11}^i)^3G_{21}^i-(M_{12}^i)^3G_{22}^i-(M_{13}^i)^3G_{23}^i-(M_{14}^i)^3G_{24}^i-F_{21}^i-F_{22}^i+F_{23}^i+F_{24}^i,$$

$$Q_3^i = M_{11}^i\left(-G_{31}^i+\frac{4}{3}G_{11}^i\right)-M_{12}^i\left(G_{32}^i-\frac{4}{3}G_{12}^i\right)-M_{13}^i\left(G_{33}^i+\frac{4}{3}G_{13}^i\right)$$
$$+M_{14}^i\left(-G_{34}^i-\frac{4}{3}G_{14}^i\right)+\frac{4}{3}F_{11}^i+\frac{4}{3}F_{12}^i,$$
$$Q_4^i = 3(-M_{11}^iG_{31}^i-M_{12}^iG_{32}^i-M_{13}^iG_{33}^i-M_{14}^iG_{34}^i),$$
$$Q_5^i = M_{21}^iM_{31}^iG_{31}^i+M_{22}^iM_{32}^iG_{32}^i+M_{23}^iM_{33}^iG_{33}^i+M_{24}^iM_{34}^iG_{34}^i,$$
$$Q_6^i = -(F_{31}^iM_{31}^i+F_{32}^iM_{32}^i+F_{33}^iM_{33}^i+F_{34}^iM_{34}^i),$$
$$Q_7^i = F_{41}^i+M_{41}^i(M_{11}^i-M_{13}^i)+M_{42}^i(-M_{12}^i+M_{14}^i),$$
$$Q_8^i = F_{51}^iM_{12}^i+F_{52}^iM_{13}^i+F_{61}^iM_{31}^i+F_{62}^iM_{34}^i+G_{41}^i-G_{42}^i+G_{43}^i-G_{44}^i,$$
$$Q_9^i = \frac{1}{2}(-G_{41}^i+G_{42}^i-G_{43}^i+G_{44}^i)-M_{51}^i+M_{52}^i+M_{53}^i-M_{54}^i, \tag{B2}$$

where F_{kl}^i, G_{kl}^i and M_{kl}^i are the fundamental functions listed below:

$$F_{11}^i = \frac{4bs_iz}{(d-y)^3},\quad F_{12}^i = \frac{4bs_iz}{(d+y)^3},\quad G_{11}^i = \frac{(-b+z)}{(d-y)^3},$$
$$G_{12}^i = \frac{(-b+z)}{(d+y)^3},\quad G_{13}^i = \frac{(b+z)}{(d-y)^3},\quad G_{14}^i = \frac{(b+z)}{(d+y)^3},$$
$$M_{11}^i = \sqrt{s_i^2(b-z)^2+(d-y)^2},\quad M_{12}^i = \sqrt{s_i^2(b-z)^2+(d+y)^2},$$
$$M_{13}^i = \sqrt{s_i^2(b+z)^2+(d-y)^2},\quad M_{14}^i = \sqrt{s_i^2(b+z)^2+(d+y)^2},$$
$$G_{21}^i = \frac{1}{3s_i^2(d-y)^3(b-z)},\quad G_{22}^i = \frac{1}{3s_i^2(d+y)^3(b-z)},$$
$$G_{23}^i = \frac{1}{3s_i^2(d-y)^3(b+z)},\quad G_{24}^i = \frac{1}{3s_i^2(d+y)^3(b+z)},$$
$$F_{21}^i = \frac{s_i(b-z)^2}{3(d-y)^3},\quad F_{22}^i = \frac{s_i(b-z)^2}{3(d+y)^3},\quad F_{23}^i = \frac{s_i(b+z)^2}{3(d-y)^3},\quad F_{24}^i = \frac{s_i(b+z)^2}{3(d+y)^3},$$
$$G_{31}^i = \frac{1}{3s_i^2(d-y)(b-z)},\quad G_{32}^i = \frac{1}{3s_i^2(d+y)(b-z)},$$
$$G_{33}^i = \frac{1}{3s_i^2(d-y)(b+z)},\quad G_{34}^i = \frac{1}{3s_i^2(d+y)(b+z)},$$
$$M_{21}^i = -2s_i^2(b-z)^2-(d-y)^2,\quad M_{22}^i = -2s_i^2(b-z)^2-(d+y)^2,$$
$$M_{23}^i = -2s_i^2(b+z)^2-(d-y)^2,\quad M_{24}^i = -2s_i^2(b+z)^2-(d+y)^2,$$
$$M_{31}^i = \frac{1}{\sqrt{s_i^2(b-z)^2+(d-y)^2}},\quad M_{32}^i = \frac{1}{\sqrt{s_i^2(b-z)^2+(d+y)^2}},$$
$$M_{33}^i = \frac{1}{\sqrt{s_i^2(b+z)^2+(d-y)^2}},\quad M_{34}^i = \frac{1}{\sqrt{s_i^2(b+z)^2+(d+y)^2}},$$
$$M_{51}^i = \frac{(d-y)^2+2s_i^2(b-z)^2}{s_i(d-y)^2\sqrt{s_i^2(b-z)^2+(d-y)^2}},$$
$$M_{52}^i = \frac{(d+y)^2+2s_i^2(b-z)^2}{s_i(d+y)^2\sqrt{s_i^2(b-z)^2+(d+y)^2}},$$
$$M_{53}^i = \frac{(d-y)^2+2s_i^2(b+z)^2}{s_i(d-y)^2\sqrt{s_i^2(b+z)^2+(d-y)^2}},$$
$$M_{54}^i = \frac{(d+y)^2+2s_i^2(b+z)^2}{s_i(d+y)^2\sqrt{s_i^2(b+z)^2+(d+y)^2}},$$
$$F_{31}^i = \frac{d-y}{s_i^2(b-z)},\quad F_{32}^i = \frac{d+y}{s_i^2(b-z)},$$
$$F_{33}^i = \frac{d-y}{s_i^2(b+z)},\quad F_{34}^i = \frac{d+y}{s_i^2(b+z)},$$
$$F_{41}^i = \frac{8bdy}{(d-y)^2(d+y)^2},\quad M_{41}^i = \frac{1}{s_i(d-y)^2},\quad M_{42}^i = \frac{1}{s_i(d+y)^2},$$
$$F_{51}^i = \frac{1}{s_i(d+y)^2}\left(-4+\frac{(d+y)^2}{(d+y)^2+s_i^2(b-z)^2}\right),$$
$$F_{52}^i = \frac{1}{s_i(d-y)^2}\left(-4+\frac{(d-y)^2}{(d-y)^2+s_i^2(b+z)^2}\right),$$
$$G_{41}^i = \frac{4(b-z)}{(d-y)^2},\quad G_{42}^i = \frac{4(b-z)}{(d+y)^2},\quad G_{43}^i = \frac{4(b+z)}{(d-y)^2},\quad G_{44}^i = \frac{4(b+z)}{(d+y)^2},$$
$$F_{61}^i = \frac{3(d-y)^2+4s_i^2(b-z)^2}{s_i(d-y)^2},\quad F_{62}^i = \frac{3(d+y)^2+4s_i^2(b+z)^2}{s_i(d+y)^2}. \tag{B3}$$

References

[1] Yang W.Mechanics and reliability of actuating materials. In: Proceedings of IUTAM-symposium Beijing 2004. Dordrecht: Springer; 2006.
[2] Trolier-McKinstry S, Newnham RE. Sensors, actuators, and smart materials. J MRS Bull 1993:27–33.
[3] Alshits VI, Kircher HOK, Ting TCT. Angularly inhomogeneous piezoelectric piezomagnetic magnetoelastic anisotropic media. Philos Mag Lett 1995:285–8.
[4] Suo Z, Kuo C-M, Barnett DM, Willis JR. Fracture mechanics for piezoelectric ceramics. J Mech Phys Solids 1992:739–65.
[5] Sih GC, Zuo JZ. Multiscale behavior of crack initiation and growth in piezoelectric ceramics. Theor Appl Fract Mech 2000:123–41.
[6] Zhang TY, Zhao MH, Tong P. Fracture of Piezoelectric Ceramics. Adv Appl Mech 2002:147–289.
[7] Qin QH. Fracture mechanics of piezoelectric materials. Southampton: WIT Press; 2001.
[8] Liu TJC. Anomalies associated with energy release parameters for cracks in piezoelectric materials. Theor Appl Fract Mech 2009:102–10.
[9] Zhang T-Y, Gao CF. Fracture behaviors of piezoelectric materials. Theor Appl Fract Mech 2004:339–79.
[10] Kuna M. Fracture mechanics of piezoelectric materials—where are we right now? Eng Fract Mech 2010:309–26.
[11] Beom HG, Jeong KM, Park JY, Lin S, Kim GH. Electrical failure of piezoelectric ceramics with a conductive crack under electric fields. Eng Fract Mech 2009:2399–407.
[12] Chue CH, Weng SM. Fracture analysis of piezoelectric materials with an arbitrarily oriented crack using energy density theory. Comput Struct 2005:1251–65.
[13] Banks-Sills L, Motola Y, Shemesh L. The *M*-integral for calculating intensity factors of an impermeable crack in a piezoelectric material. Eng Fract Mech 2008:901–25.
[14] Motola Y, Banks-Sills L, Fourman V. On fracture testing of piezoelectric ceramics. Int J Fract 2009:167–90.
[15] Sih GC. A field model interpretation of crack initiation and growth behavior in ferroelectric ceramics: change of poling direction and boundary condition. Theor Appl Fract Mech 2002:1–14.
[16] Sosa HA, Pak YE. 3-dimensional eigenfunction analysis of a crack in a piezoelectric material. Int J Solids Struct 1990:1–15.
[17] Yang JH, Lee KY. Penny shaped crack in a three-dimensional piezoelectric strip under in-plane normal loadings. Acta Mech 2001:187–97.
[18] Chen WQ, Ding HJ, Xu RQ. Three-dimensional static analysis of multi-layered piezoelectric hollow spheres via the state space method. Int J Solids Struct 2001:4921–36.
[19] Chen MC. Application of finite-part integrals to three-dimensional fracture problems for piezoelectric media—Part I: Hypersingular integral equation and theoretical analysis. Int J Fract 2003:133–48.
[20] Hwu C, Ikeda T. Electromechanical fracture analysis for corners and cracks in piezoelectric materials. Int J Solids Struct 2008:5744–64.
[21] Zhao MH, Shen YP, Liu YJ, Liu GL. Isolated crack in three-dimensional piezoelectric solid: Part I: Solution by Hankel transform. Theor Appl Fract Mech 1997:129–39.
[22] Zhao MH, Shen YP, Liu YJ, Liu GL. Isolated crack in three-dimensional piezoelectric solid: Part II: Stress intensity factors for circular crack. Theor Appl Fract Mech 1997:141–9.
[23] Zhao MH, Shen YP, Liu GN, et al. Dugdale model solutions for a penny-shaped crack in three-dimensional transversely isotropic piezoelectric media by boundary-integral equation method. Eng Anal Bound Elem 1999:573–6.
[24] Zhao MH, Li N, Fan CY. Solution method of interface cracks in three-dimensional transversely isotropic piezoelectric bimaterials. Eng Anal Bound Elem 2008:545–55.
[25] Zhao MH, Yang F, Liu T, et al. Boundary integral equation method for conductive cracks in two and three-dimensional transversely isotropic piezoelectric media. Eng Anal Bound Elem 2005:466–76.
[26] Zhao MH, Fang PZ, Shen YP. Boundary integral-differential equations and boundary element method for interfacial cracks in three-dimensional piezoelectric media. Eng Anal Bound Elem 2004:753–62.
[27] Crouch SL. Solution of plane elasticity problems by the displacement discontinuity method. Int J Numer Methods Eng 1976:301–43.
[28] Zhao MH, Liu YJ, Cheng C. Boundary-integral equations and the boundary-element method for three-dimensional fracture mechanics. Eng Anal Bound Elem 1994:333–8.
[29] Pan E, Yuan FG. Boundary element analysis of three-dimensional cracks in anisotropic solids. Int J Numer Methods Eng 2000:211–37.
[30] Pan EA. BEM analysis of fracture mechanics in 2D anisotropic piezoelectric solids. Eng Anal Bound Elem 1999:67–76.

[31] Qin TY, Yu YS, Noda NA. Finite-part integral and boundary element method to solve three-dimensional crack problems in piezoelectric materials. Int J Solids Struct 2007:4770–83.
[32] Zhao MH, Xu GT, Fan CY. Hybrid extended displacement discontinuity-charge simulation method for analysis of cracks in 2D piezoelectric media. Eng Anal Bound Elem 2009:592–600.
[33] Fan CY, Zhao MH, Zhou YH. Numerical solution of polarization saturation/dielectric breakdown model in 2D finite piezoelectric media. J Mech Phys Solids 2009:1527–44.
[34] Hill LR, Farris TN. Three-dimensional piezoelectric boundary element method. AIAA J 1998:102–8.
[35] Zhao MH, Fan CY, Liu T, Yang F. Extended displacement discontinuity Green's functions for three dimensional transversely isotropic magneto-electro-elastic media and applications. Eng Anal Bound Elem 2007;31(6):547–58.
[36] Ding HJ, Chen WQ, Jiang AM. Green's functions and boundary element method for transversely isotropic piezoelectric materials. Eng Anal Bound Elem 2004:975–87.
[37] Wang XM, Shen YP. Theorem of work reciprocity for pyroelectric elastic media with application. Acta Mech Sin 1996;28(2):244–50.
[38] Kassier MK, Sih GC. Three-dimensional crack problems. Mechanics of fracture II. Boston, Leyden: Noordhoff International Publishing (Kluwer Academic Publishers); 1975.